Chemical Science

EDGE ARTICLE

View Article Online
View Journal | View Issue

Cite this: *Chem. Sci.*, 2016, **7**, 2257

Nucleic acid-selective light-up fluorescent biosensors for ratiometric two-photon imaging of the viscosity of live cells and tissues†

Dandan Li,‡[a] Xiaohe Tian,‡[b] Aidong Wang,[c] Lijuan Guan,[d] Jun Zheng,[a] Fei Li,[a] Shengli Li,[a] Hongping Zhou,[a] Jieying Wu[a] and Yupeng Tian*[a]

Received 19th October 2015
Accepted 14th December 2015

DOI: 10.1039/c5sc03956h

www.rsc.org/chemicalscience

Rational design of specific ratiometric viscosity probes with small molecular weight is a challenge in practical biotechnology applications. Herein two novel water-soluble, small-molecular ratiometric probes, bearing *N*-methyl benzothiazolium moiety (DSF and DBF), are designed for two-photon fluorescent imaging as a functional of local viscosity. The dye DSF, a light-up fluorescent probe, is sensitive to local viscosity and selectively stains nuclear DNA, which can be used to inspect asynchronous cells under confocal microscopy. While the dye DBF as a molecular rotor displays strong fluorescence enhancement in viscous media or binding to RNA. It exhibits dual absorption and emission as well, and only the red emission is markedly sensitive to viscosity changes, providing a ratiometric response and selectively imaging nucleolic and cytosolic RNA. Interestingly it is shown, for the first time, that the intracellular targeting and localization (DNA and RNA) of the two dyes are entirely realized simply by modifying the substituent attached to the benzothiazolium.

Introduction

The character of each component in a cellular system and their complex biological functions and processes has attracted increasing attention, and therefore better understanding of the selective staining/imaging of specific cellular organelles is of paramount importance.[1] Since nucleic acid (NA) including DNA and RNA is the major source for storing, duplicating and transferring the genetic information in all eukaryotic cells,[2,3] design tools in NA imaging have become of great interest.[4–7] Commercial nuclear imaging agents[8] such as DAPI, Hoechst 33342 (DNA) and SYTO-Select (RNA) probe require ultraviolet light as excitation source, resulting in significant autofluorescence and extensive photon toxicity.[9,10] An attractive approach for the selective detection of NA in living samples is ratiometric imaging with two-photon microscopy (TPM). The former offers quantitative measurement and avoids most of the interferences from microenvironments; the latter gives deeper tissue penetration and an autofluorescence-free background.[11–18] However, ratiometric two-photon absorption molecules generally possess large π-conjugated systems, resulting in relatively large molecular weight, and involve extensive synthesis procedures.[19–24] Therefore, NA-specific ratiometric two-photon excited fluorescence (TPEF) probes with optimized two-photon action cross-section ($\Phi\delta$) and appropriate biocapability (*e.g.* aqueous solubility, membrane permeability) are the next ideal image systems.

Viscosity strongly influences intracellular substance transportation, biomacromolecule interactions, and reactive metabolite diffusion in live cells,[25] and consequently abnormal viscosity variations strongly reflect many diseases and malfunctions.[26–30] In recent years, "molecular rotors", microviscosity-targeted fluorescent sensors, have gradually emerged with the application of fluorescence technology.[31–36] Nevertheless, these sensors are unable to quantitatively determine intracellular microviscosity or its variations due to the influence of experimental and instrumental factors. Therefore, novel molecular rotors with dual emission maxima capable of quantifying viscosity[37–41] in living samples and avoiding most of the interferences are indeed in demand.

Considering the above, two water-soluble small organic molecules with optimized two-photon action cross-section were designed. The introduction of *N*-methyl benzothiazolium moiety (as an acceptor A) and the ease of modifying the substituent attached to the benzothiazolium result in strong and concomitant optimization of both optical performances and NA binding parameters. A 2-(methylamino)ethanol unit

[a]*Department of Chemistry, Anhui University, Hefei, China. E-mail: yptian@ahu.edu.cn*
[b]*School of Life Science, Anhui University, Hefei, China*
[c]*Huangshan University, Huangshan, China*
[d]*Department of Chemistry, University College London, London, UK*

† Electronic supplementary information (ESI) available: The detailed synthetic processes, fully characterizations of the two dyes. The crystal structural and DNA binding information of DSF. The water solubility, pH effect, cytotoxicity and photostability of DSF and DBF. CCDC 1432097. For ESI and crystallographic data in CIF or other electronic format see DOI: 10.1039/c5sc03956h

‡ These authors contributed equally.

acts as a donor (D) and its HO– group should tend to form strong hydrogen bonds with the other polar molecules around its microenvironment. It was found that a minor modification of the substituent attached to the benzothiazolium significantly alters the final subcellular destination. Consequently, this led to the identification of two novel TPEF probes called DSF and DBF having high affinity binding to nuclear DNA and intracellular RNA, respectively. Importantly, inside living cells and tissues, the viscosity changes, showing some regional difference, can be clearly observed by ratiometric two-photon imaging using two such probes. This is the first time that two 2PA fluorescent agents, which also offer *in situ* intracellular viscosity quantitation, have been applied to image DNA and RNA in living cells and tissues.

Results and discussion

Experimental

One-photon excited fluorescence response to solvent viscosity. Generally solvents with different polarity influence wavelengths and quantum yields to some extent. However, as shown in Fig. 1a and d, the quantum yield (QY) of DSF or DBF was very low in low-viscosity solvents, and apparently was not affected by solvent polarity. On the other hand, DSF and DBF showed a sharp fluorescence enhancement with increasing solvent viscosity. As glycerol was gradually added to the solvent mixture, the viscosity of the solutions increased from 1.0 cP (water) to approximately 950 cP (99% glycerol), and consequently the fluorescence of DSF and DBF increased 19-fold (QY = 0.27) and 16-fold (QY = 0.35) in 99% glycerol, respectively.

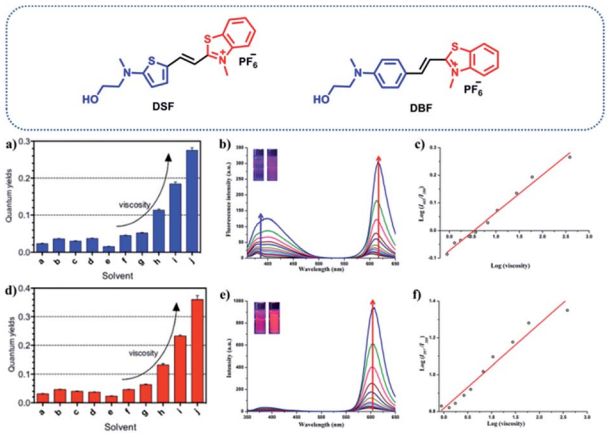

Fig. 1 The fluorescence quantum yields of (a) DSF (λ_{ex} = 560 nm) and (d) DBF (λ_{ex} = 505 nm) in different solvents: (a) dichloromethane, (b) DMSO, (c) ethanol, (d) methanol, (e) water, (f) water/glycerol (8 : 2 v/v), (g) water/glycerol (6 : 4 v/v), (h) water/glycerol (4 : 6 v/v), (i) water/glycerol (2 : 8 v/v), (j) glycerol (99%). Changes in the fluorescence emission spectra of (b) DSF and (e) DBF as a function of the solvent viscosity (excited at 335 nm). Insets: photographs taken under UV illumination of DSF and DBF in water (left) and 99% glycerol (right), respectively. The linear response between log($I_{605\ nm}/I_{380\ nm}$) for (c) DSF and log($I_{597\ nm}/I_{380\ nm}$) for (f) DBF and log(viscosity) in the water/glycerol solvent (excited at 335 nm).

This is crucial to permit a molecular rotor to reflect environmental viscosity.[42]

To further investigate their utility as molecular rotors for quantifying viscosity, the changes of fluorescence emission spectra for DSF and DBF as a function of the solvent viscosity were investigated. As illustrated in Fig. S3,† DSF exhibits two emission bands in aqueous solution. The red-emission band (λ_{em}(red) = 605 nm) increased much faster than the blue-emission band (λ_{em}(blue) = 380 nm) as the viscosity of the solution increased (Fig. 1b). In addition, the logarithm of the fluorescence ratio thereof ($I_{605\ nm}/I_{380\ nm}$) has a linear relationship with that of the viscosity (η) of the solution, which is as expected from the Förster–Hoffmann equation:[43]

$$\log I_f = C + x \log \eta$$

where C is a concentration that is temperature-dependent and x is a dye-dependent constant. Therefore, log($I_{605\ nm}/I_{380\ nm}$) of DSF and log η were plotted accordingly (Fig. 1c, R^2 = 0.99, slope x = 0.14). In addition, similar to DSF, DBF possesses a unique spectral character, with two emission peaks (such as λ_{em} = 380 and 597 nm in water, Fig. S3†). Most importantly, only the red emission of DBF responded significantly to the viscosity of the solvent. As shown in Fig. 1e, with increasing proportions of glycerol in the solvent mixture, the red fluorescence intensity at 597 nm increased sensitively with viscosity of the solvent. The blue emission at 380 nm, however, gave only very small responses. This permits ratiometric changes with a linear relationship between log(I_{597}/I_{380}) and log η, which is fitted by the Förster–Hoffmann equation. R^2 of the linear relation increases in the water–glycerol system (Fig. 1f) was 0.96, and the slope x was 0.23. This indicated that DSF and DBF could be applied as ratiometric sensors to quantitatively detect the solution viscosity.

Two-photon absorption response to solvent viscosity. Stilbazolium salts with D–π–A molecular configuration have been reported to have two-photon properties.[44–46] As shown in Fig. 2, the two-photon absorption spectra of DSF and DBF changed significantly with a rise in solvent viscosity. The two-photon action cross-section ($\Phi\delta$) at 720 nm of DSF increased from 5.0 (water) to 75.6 GM (99% glycerol) and $\Phi\delta$ at 800 nm of DBF increased from 9.0 (water) to 98.8 GM (99% glycerol) (1 GM = 10^{-50} cm^4 s photon^{-1}). Their reasonable two-photon action cross-sections are the attractive features for their utility as biological probes.

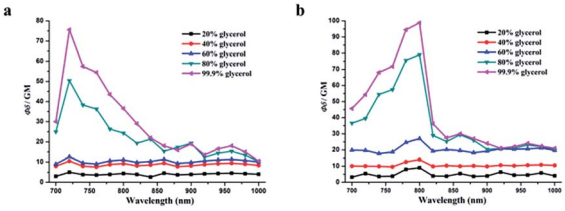

Fig. 2 Two-photon (TP) action cross-section spectra of (a) DSF (0.1 mM) and (b) DBF (0.1 mM) in solvents of varying viscosity. TP excitation: 700–1000 nm.

The cellular uptake properties of DSF and DBF. Considering the comprehensive merits of the dyes, biological imaging application of DSF and DBF was carried out using HepG2 cells (liver hepatocellular carcinoma) as a model. Initially their cytotoxicity and photon resistance abilities were evaluated *via* standard MTT assay and photon bleaching experiments (Fig. S7†). The results suggested the noninvasiveness at even high concentration (25 μM) and strong photon resistance against laser irradiation (150 s), making feasible further studies in living samples.

Cell localization of DSF: a DNA-specific luminescent cellular imaging agent. Cell-staining experiments using two-photon confocal microscopy showed that DSF (10 μM, 30 min) could readily enter living HepG2 cells effectively and predominantly emission is apparently observed from the cell nucleus (Fig. 3a). Furthermore, DSF visualizes characteristic structural changes in nuclear DNA as cells progress through the cell cycle. As shown in higher resolution micrographs (Fig. 3b) of single cells, when asynchronous cells are imaged, the majority of labelled cells are interphase but cells undergoing mitotic phases are also clearly observed. Notably, cells undergoing interphase with dense chromosomes (Fig. 3a, white arrows) obviously displayed a brighter signal as an indication of local DNA viscosity. To the best of our knowledge, DNA-specific 2PA luminescent cellular imaging probes, which can be used to inspect asynchronous cells by cell imaging, are extremely rare.[47,48]

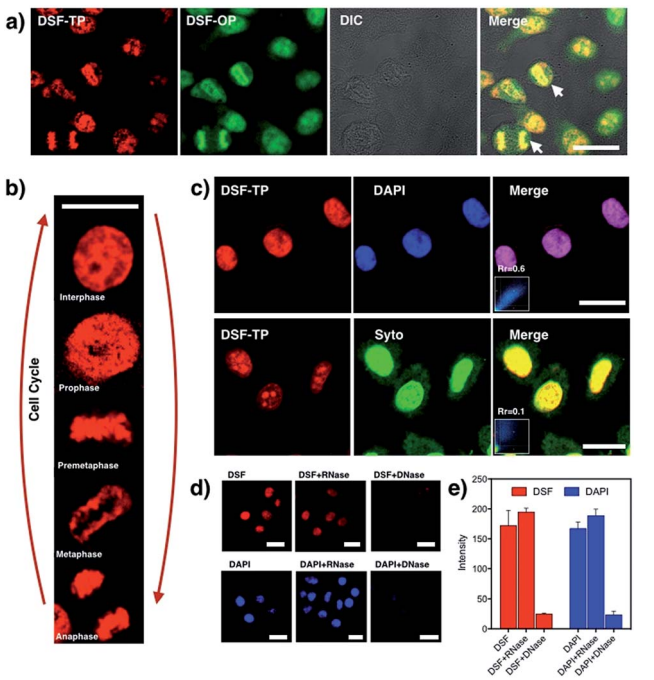

Fig. 3 Fluorescent images of living cells by DSF. (a) One- and two-photon excitation were at 488 and 720 nm, respectively: OPM image of DSF (580–620 nm), TPM image of DSF (590–630 nm). (b) Asynchronous cell imaging shows mitotic cells stained by DSF visualizing chromosome aggregation through progression of mitosis. (c) Co-staining of DSF (red, TPM: λ_{ex} = 720 nm) with DNA-specific dye DAPI (blue) and general nucleic acid dye SYTO 9 (green). (d) DNase and RNase digest experiments of DSF (TPM: λ_{ex} = 720 nm) and DAPI (shown as comparison experiments). (e) The intensity of fluorescent images for DNase and RNase digest experiments. Scale bar: 20 μm.

To establish the precise intracellular localization of DSF, co-staining experiments were performed. Incubation of HepG2 cells with DSF and co-staining with the membrane-permeable DAPI, a DNA minor-groove binder, shows strong co-localization of the two emission signals (Fig. 3c; Pearson's correlation coefficient: R_r = 0.60). Conversely, co-staining with SYTO 9, a general nucleic acid stain, shows a clear difference in localization (R_r = 0.10). In addition, deoxyribonuclease (DNase) and ribonuclease (RNase) digest experiments were also performed (Fig. 3d and e) to identify the species stained by DSF in the nucleus, while DAPI was also tested as control. Upon treatment with RNase, no significant loss of fluorescence in the nucleus occurred for DSF. By contrast, after DNase digestion, the nuclear fluorescence signals of DSF were completely lost. DSF exhibited a similar behavior in the digest experiment with DAPI, indicating that nuclear fluorescence originated from the binding of DSF with DNA in the nucleus. DNase/RNase digest experiments and co-staining with other commercially available fluorescent nuclear stains reveal that DSF is clearly targeting nuclear DNA in live cells.

Cell localization of DBF: imaging of RNA-rich nucleolus and RNA in cytoplasm. In a parallel experiment, a living cell sample was incubated with 10 μM DBF for 30 min. As shown in Fig. S10A,† the green fluorescence mainly localizes at the cytoplasm and nucleoli accompanied with faint nuclei distribution. In addition, TPM has revolutionized the biological sciences by enabling non-invasive, high-resolution imaging of living samples in real time. Therefore, to confirm the fluorescence spots observed in the nucleolus, the two-photon fluorescence images and DIC pictures were compared (Fig. S10B†), and bright fluorescence spots just coincide with nucleoli, the densest and phase-dark region of the nucleus. In addition, co-staining experiments were performed (Fig. 4a). The DBF signal showed strong overlap with SYTO 9 (R_r = 0.76). Conversely, the co-localization profile showed minimal overlapping between DBF and DAPI (R_r = 0.34).

As is well known, the nucleolus contains abundant RNAs and proteins, especially ribosomal RNA and ribosomal proteins. To investigate the selectivity for RNA of DBF in cells, a digest test of RNase, which only hydrolyzes the RNA in the cell and does not influence the DNA, was performed (Fig. 4b). The only commercial RNA probe, SYTO RNA-Select, was also used as control. From Fig. 4b, the same as SYTO RNA-Select, in contrast to the untreated samples, the fluorescence of DBF in cytoplasm and nucleoli dramatically diminished and tended to redistribute to the nucleoli. In addition, upon treatment with DNase, no significant loss of fluorescence in the nucleus occurred for DBF and SYTO RNA-Select (Fig. 4c). The result indicates that DBF can selectively stain RNA in the nucleolus and cytoplasm, which would be of great advantage in the observation of RNA content and distribution and the visualization of nucleolus-related events.

Ratiometric two-photon fluorescence cell and tissue imaging. Since DSF and DBF could be applied with the fluorescence-enhancement method that senses viscosity change,

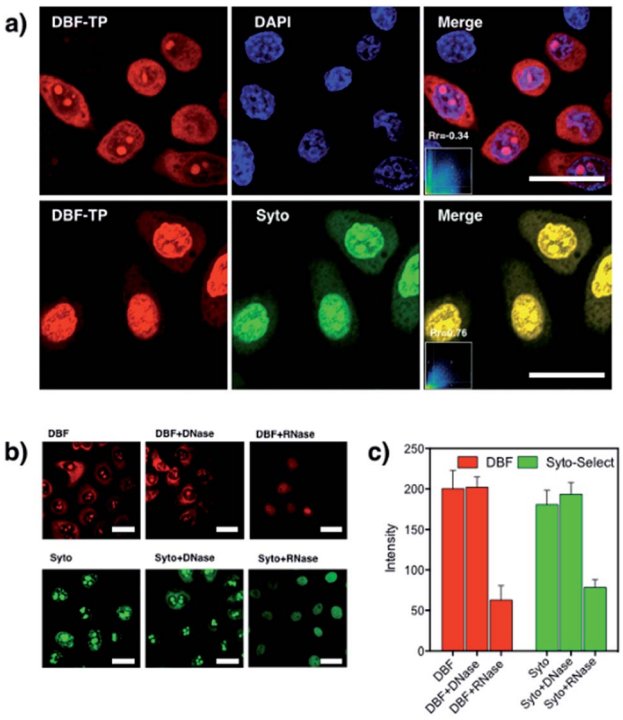

Fig. 4 (a) Co-staining of DBF (red, TPM: λ_{ex} = 800 nm) with DNA-specific dye DAPI (blue) and general nucleic acid dye SYTO 9 (green). (b) DNase and RNase digest experiments of DBF (TPM: λ_{ex} = 800 nm) and SYTO 9. (c) The intensity of fluorescent images for DNase and RNase digest experiments. Scale bar: 20 μm.

the two NA sensors with two emission peaks can be also applied to the ratiometric fluorescence imaging of viscosity in live cells. Excited at 720 nm for DSF and 800 nm for DBF, the fluorescence images were obtained by collecting the blue emission of 375–450 nm (green channel) and the red emission of 570–650 nm (red channel) (Fig. 5). The ratio image ($I_{605\ nm}/I_{380\ nm}$) of DSF and ($I_{597\ nm}/I_{380\ nm}$) clearly displayed the distribution of viscosity in the cells (left, Fig. 6). In addition, due to their 2PA property, we further investigated the application of these sensors in thick tissue imaging (>200 μm) *ex vivo*. A fresh rat liver slice incubated with 10 μM DSF or DBF for 30 min not only

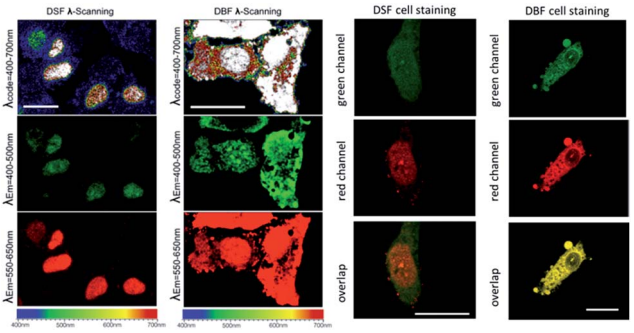

Fig. 5 Live HepG2 cell staining with DSF (10 μM, 30 min incubation, excited at 720 nm) and DBF (10 μM, 30 min incubation excited at 800 nm): green channel (375–450 nm), red channel (570–650 nm). Scale bar: 20 μm.

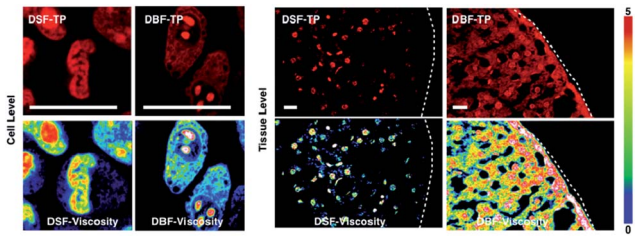

Fig. 6 Live HepG2 cell and fresh rat liver slice staining with DSF (10 μM, 30 min incubation, excited at 720 nm) and DBF (10 μM, 30 min incubation excited at 800 nm), red channel (570–650 nm), the ratio image of DSF and DBF obtained with ImageJ software.

showed DNA/RNA labeling but also offered viscosity distribution (Fig. 6, right): the "blue" regions, indicating the viscosity is less than 100 cP, and the "green" imaging areas represent an intermediate viscosity of cell and tissue slice (100–500 cP). Some small intracellular red zones indicate high viscosity (about 900 cP) in living samples.

The above results showed that the two NA sensors as two-photon ratiometric rotors could be used to probe viscosity changes *in vitro* and *ex vivo* by ratiometric two-photon imaging. Additionally, the two rotors with dual emission maxima are capable of quantifying viscosity in cells and tissues, avoiding most of the interferences from the fluid optical properties, dye concentration, and other experimental or instrumental factors.

Possible influencing factors on targeting and localization properties. To further investigate the DSF preference to DNA and DBF preference to RNA *in vitro*, the interactions of dyes DSF and DBF with numerous substances in the nucleus, including various amino acids, peptides, deoxyribonucleotide (dNTP), proteins, DNA, and RNA, were examined by absorption and fluorescence spectra. As shown in Fig. S11 and Table S3,† the observation of hypochromism in the absorption spectra is due to the stacking interactions between the aromatic ring and the base pairs of DNA.[49] Meanwhile, the addition of DNA to DSF triggered a pronounced bathochromic effect in absorption spectra and a significant luminescence enhancement ("light-switch" effect, Fig. S11B†) while other biological molecules do not give rise to such an effect, which reveals the strong interaction between DSF and DNA, in agreement with the initial cell-staining experiments. In addition, as Fig. S11C† shows, upon addition of NA (DNA and RNA), a pronounced bathochromic effect in absorption spectra is observed for DBF, which reveals the strong interaction between DBF and NA. The fluorescence intensity of DBF upon interaction with RNA displays a larger fluorescence enhancement than DNA for the same amount of NA (Fig. S11D†). A similar phenomenon for SYTO RNA-Select was also observed in reported works,[50] indicating that DBF and SYTO RNA-Select both have higher response to RNA than to DNA. While the cell-staining experiments indicate DBF selectively stains RNA in cells, and this puzzling state is possibly due to the difference between the structure of NAs in solution and their real state in cells and specific interaction between different probes and NAs.[51] Accordingly, the weak emission of DSF and DBF in water can be attributed to the strong interaction of the

molecules in the excited state with the water environment, which induces the formation of twisting intramolecular charge transfer state, resulting in the increase of non-radiative decay. The luminescence enhancement of dyes DSF and DBF on binding to NA could be explained by two factors: firstly, the immobilization that reduces non-radiative processes associated with molecular internal rotation around the vinyl bond; secondly, the screening from water once the dyes are inserted inside NA.[52]

Considering that DSF and DBF both can bind to DNA, to understand more thoroughly the sequence selectivity of them, we studied them in the presence of the polynucleotides poly(dA-dT)$_2$ and poly(dG-dC)$_2$. As shown in Fig. S12,† the increase in fluorescence of DSF/DBF in the presence of the former is higher than the latter which is due to the AT displaying a more negative electrostatic potential as compared to other sequences, which is favorable to cation trapping.[4] On the basis of the data discussed above, we conducted molecular modeling calculations[53] using Discovery Studio 4.1 with duplex DNA fragment (duplex AT-rich DNA, base sequences CTTTTGCAAAAG/CTTTTGCAAAAG). The docking results (Fig. 7) indicate that DSF and DBF can bind to duplex DNA by intercalating DNA *via* the hydrogen bonding interactions of nucleobases (preferably to A ≡ T, which is in agreement with the results of fluorescence spectra change of DSF/DBF in the presence of polynucleotides poly(dA-dT)$_2$ and poly(dG-dC)$_2$). In addition, as shown in Table S4,† DSF binds to DNA with higher affinity (lower CDOCKER energy) which might be due to DSF interacting with the base pairs of DNA *via* hydrogen bonds in different directions (Fig. S14†), resulting in DSF being inserted inside DNA in a stable configuration. While, as shown in Fig. S15,† DBF interacts with the base pairs of DNA by hydrogen bonds in the same direction and in the action of the same force field, so the structure of DBF binding to DNA will be twisted.

The knowledge of the interaction mechanism between RNA and fluorescent probes is still not enough compared with the much deeper understanding of DNA biosensors. Besides, compared to the many fluorescent probes imaging DNA, the mechanisms of RNA probes for cell imaging are rarely reported.

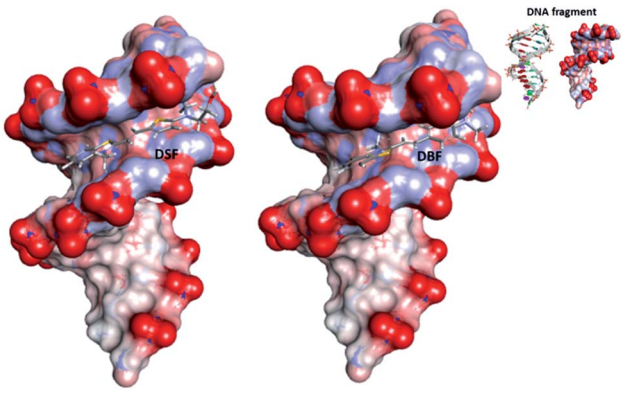

Fig. 7 Models obtained after molecular modeling of the interaction of DSF and DBF with DNA fragment. Inset: the structure of the corresponding DNA fragment.

Molecular Probes Co., which sells various DNA probes such as DAPI, series of Hoechsts, and propidium iodide, only offers the classical commercial RNA probe "SYTO RNA-Select" for imaging RNA in living cells, but its chemical structure has not been described. Also, it is not very clear why just by changing the linker thiophene (DSF) to phenyl (DBF) the binding selectivity changes from DNA to RNA. Considering the results of molecular modeling calculations for DBF and DNA fragment, it is tentatively suggested that the difference may be due to the fact that (i) some specificity of intracellular distribution and organization of RNA and DNA molecules can cause a difference in the affinity of dye DSF or DBF to DNA and RNA inside cells and (ii) DBF interacts with the base pairs of RNA by hydrogen bonds in the same direction (similar to DNA binding) and in the action of the same force field, and the structure of DBF binding to RNA will be twisted into stable crescent-shape configuration. DBF exhibits much stronger binding affinity toward RNA than DNA in a buffer solution and selectively stains and targets RNA in cells which might be attributable to crescent-shape molecules with positive charges preferring binding with RNA.[54,55] As mentioned above, DSF is clearly targeting nuclear DNA and DBF selectively stains RNA in living cells. Because of the ease of modifying the substituent attached to the thiazole, the intracellular targeting and localization properties of the two dyes are entirely different. These findings suggest that a variation of substituent attached to the benzothiazolium moiety can greatly vary the binding interaction with NA and thus provide a tool to fine-tune the targeting and localization properties of organic molecules as effective organelle-specific TPEF probes.

Conclusions

In summary, two water-soluble small organic ratiometric molecules with optimized two-photon action cross-section were developed. Because of the ease of modifying the substituent attached to the benzothiazolium moiety, the targeting and localization properties can be easily tuned and optimized for the organic molecules as effective organelle-specific TPEF probes. The two novel TPEF probes called DSF and DBF bind to nuclear DNA and RNA in the nucleolus and cytoplasm with high affinity, respectively. Importantly, the two unique fluorescent nucleic acid light-up probes as two-photon ratiometric rotors can be used for quantifying and imaging intracellular viscosity in living cells and tissues. Their advantages of exclusive NA-selective staining of living cells, high signal ratio, excitation with NIR light, good photostability, as well as low cytotoxicity at imaging concentration, promise potential applications of DSF and DBF in biological and biomedical research.

Acknowledgements

This work was supported by the National Natural Science Foundation of China (21271004, 51372003, 51432001, 21271003, 51472002 and 51402001), Focus on returned overseas scholar of Ministry of Education of China, the Higher Education Revitalization Plan Talent Project (2013), and Anhui University Doctor Startup Fund (J01001962). The work of molecular

modeling calculations on Discovery Studio (*Dassault Systèmes BIOVIA, Discovery Studio Modeling Environment, Release 4.5, San Diego: Dassault Systèmes, 2015*) was contributed by Professor Aidong Wang from Huangshan University, China.

Notes and references

1 I. B. Buchwalow and W. Böcker, *Immunohistochemistry: Basics and Methods*, Springer, Berlin, 2010.
2 A. Z. Medvedev, *Adv. Gerontol. Res.*, 1964, **21**, 181–206.
3 J. Brachet, *Prog. Biophys. Mol. Biol.*, 1965, **15**, 95–127.
4 B. Dumat, G. Bordeau, E. Faurel-Paul, F. Mahuteau-Betzer, N. Saettel, G. Metge, C. Fiorini-Debuisschert, F. Charra and M. P. Teulade-Fichou, *J. Am. Chem. Soc.*, 2013, **135**, 12697–12706.
5 L. Guo, M. S. Chan, D. Xu, D. Y. Tam, F. Bolze, P. K. Lo and M. S. Wong, *ACS Chem. Biol.*, 2015, **10**, 1171–1175.
6 P. Hanczyc, B. Norden and M. Samoc, *Dalton Trans.*, 2012, **41**, 3123–3125.
7 X. Liu, Y. Sun, Y. Zhang, F. Miao, G. Wang, H. Zhao, X. Yu, H. Liu and W. Y. Wong, *Org. Biomol. Chem.*, 2011, **9**, 3615–3618.
8 Invitrogen Home pages, *A Guide to Fluorescent Probes and Labelling Technologies*, ed. R. P. Haugland, Molecular Probes, Eugene, OR, 10th edn, 2005, pp. 397–405, http://www.probes.com and http://www.invitrogen.com.
9 G. P. Pfeifer, Y. H. You and A. Besaratinia, *Mutat. Res.*, 2005, **571**, 19–31.
10 H. M. Kim and B. R. Cho, *Chem. Rev.*, 2015, **115**, 5014–5055.
11 W. R. Zipfel, R. M. Williams and W. W. Webb, *Nat. Biotechnol.*, 2003, **21**, 1369–1377.
12 F. Helmchen and W. Denk, *Nat. Methods*, 2005, **2**, 932–940.
13 R. M. Williams, W. R. Zipfel and W. W. Webb, *Curr. Opin. Chem. Biol.*, 2001, **5**, 603–608.
14 L. Guo and M. S. Wong, *Adv. Mater.*, 2014, **26**, 5400–5428.
15 H. M. Kim, B. H. Jeong, J. Y. Hyon, M. J. An, M. S. Seo, J. H. Hong, K. J. Lee, C. H. Kim, T. Joo, S. C. Hong and B. R. Cho, *J. Am. Chem. Soc.*, 2008, **130**, 4246–4247.
16 X. H. Wang, D. M. Nguyen, C. O. Yanez, L. Rodriguez, H. Y. Ahn, M. V. Bondar and K. D. Belfield, *J. Am. Chem. Soc.*, 2010, **132**, 12237–12239.
17 J. H. Han, S. K. Park, C. S. Lim, M. K. Park, H. J. Kim, H. M. Kim and B. R. Cho, *Chem.–Eur. J.*, 2012, **18**, 15246–15249.
18 W. Yang, P. S. Chan, M. S. Chan, K. F. Li, P. K. Lo, N. K. Mak, K. W. Cheah and M. S. Wong, *Chem. Commun.*, 2013, **49**, 3428–3430.
19 K. P. Divya, S. Sreejith, P. Ashokkumar, K. Yuzhan, Q. Peng, S. K. Maji, Y. Tong, H. Yu, Y. Zhao, P. Ramamurthy and A. Ajayaghosh, *Chem. Sci.*, 2014, **5**, 3469–3474.
20 L. Yuan, F. Jin, Z. Zeng, C. Liu, S. Luo and J. Wu, *Chem. Sci.*, 2015, **6**, 2360–2365.
21 C. S. Lim, G. Masanta, H. J. Kim, J. H. Han, H. M. Kim and B. R. Cho, *J. Am. Chem. Soc.*, 2011, **133**, 11132–11135.
22 S. K. Bae, C. H. Heo, D. J. Choi, D. Sen, E. H. Joe, B. R. Cho and H. M. Kim, *J. Am. Chem. Soc.*, 2013, **135**, 9915–9923.
23 H. J. Kim, C. H. Heo and H. M. Kim, *J. Am. Chem. Soc.*, 2013, **135**, 17969–17977.
24 L. Zhou, X. Zhang, Q. Wang, Y. Lv, G. Mao, A. Luo, Y. Wu, Y. Wu, J. Zhang and W. Tan, *J. Am. Chem. Soc.*, 2014, **136**, 9838–9841.
25 S. T. Ohnishi and T. Ohnishi, *Membrane Abnormalities in Sickle Cell Disease and in Other Red Blood Cell Disorders*, CRC Press, Boca Raton, Florida, 1994.
26 J. Harkness, *Biorheology*, 1971, **8**, 171–193.
27 M. J. Stutts, C. M. Canessa, J. C. Olsen, M. Hamrick, J. A. Cohn, B. C. Rossier and R. C. Boucher, *Science*, 1995, **269**, 847–850.
28 P. M. Moriarty and C. A. Gibson, *Cardiovasc. Rev. Rep.*, 2003, **24**, 321–325.
29 S. Alain, G. Jérôme, C. Gilles, M. Jean-Louis and L. Jaime, *J. Hypertens.*, 2002, **20**, 159–169.
30 I. Uchimura and F. Numano, *Diabetes Front.*, 1997, **8**, 33–37.
31 R. O. Loutfy and B. A. Arnold, *J. Phys. Chem.*, 1982, **86**, 4205–4211.
32 M. A. Haidekker, T. T. Ling, M. Anglo, H. Y. Stevens, J. A. Frangos and E. A. Theodorakis, *Chem. Biol.*, 2001, **8**, 123–131.
33 B. D. Allen, A. C. Benniston, A. Harriman, S. A. Rostron and C. Yu, *Phys. Chem. Chem. Phys.*, 2005, **7**, 3035–3040.
34 M. A. H. Alamiry, A. C. Benniston, G. Copley, K. J. Elliott, A. Harriman, B. Stewart and Y. G. Zhi, *Chem. Mater.*, 2008, **20**, 4024–4032.
35 X. Yin, Y. Li, Y. Zhu, X. Jing, Y. Li and D. Zhu, *Dalton Trans.*, 2010, **39**, 9929–9935.
36 F. Zhou, J. Shao, Y. Yang, J. Zhao, H. Guo, X. Li, S. Ji and Z. Zhang, *Eur. J. Org. Chem.*, 2011, 4773–4787.
37 H. S. Guo, P. Zhu, F. Guo, X. L. Li, X. L. Wu, X. Y. Fan, L. Wen and F. C. Tang, *Nat. Protoc.*, 2015, **10**, 645–659.
38 F. Liu, T. Wu, J. Cao, S. Cui, Z. Yang, X. Qiang, S. Sun, F. Song, J. Fan, J. Wang and X. Peng, *Chem.–Eur. J.*, 2013, **19**, 1548–1553.
39 D. Fischer, E. A. Theodorakis and M. A. Haidekker, *Nat. Protoc.*, 2007, **2**, 227–236.
40 X. Peng, Z. Yang, J. Wang, J. Fan, Y. He, F. Song, B. Wang, S. Sun, J. Qu, J. Qi and M. Yan, *J. Am. Chem. Soc.*, 2011, **133**, 6626–6635.
41 Z. Yang, J. Cao, Y. He, J. H. Yang, T. Kim, X. Peng and J. S. Kim, *Chem. Soc. Rev.*, 2014, **43**, 4563–4601.
42 M. A. Haidekker, T. P. Brady, D. Lichlyter and E. A. Theodorakis, *Bioorg. Chem.*, 2005, **33**, 415–425.
43 T. Förster and Z. G. Z. Hoffmann, *Phys. Chem.*, 1971, **75**, 63–76.
44 B. J. Coe, J. A. Harris, I. Asselberghs, K. Wostyn, K. Clays, A. Persoons, B. S. Brunschwig, S. J. Coles, T. Gelbrich, M. E. Light, M. B. Hursthouse and K. Nakatani, *Adv. Funct. Mater.*, 2003, **13**, 347–357.
45 G. S. He, J. Zhu, A. Baev, M. Samoc, D. L. Frattarelli, N. Watanabe, A. Facchetti, H. Agren, T. J. Marks and P. N. Prasad, *J. Am. Chem. Soc.*, 2011, **133**, 6675–6680.
46 Q. Zheng, H. Zhu, S. C. Chen, C. Tang, E. Ma and X. Chen, *Nat. Photonics*, 2013, **7**, 234–239.

47 M. R. Gill, J. Garcia-Lara, S. J. Foster, C. Smythe, G. Battaglia and J. A. Thomas, *Nat. Chem.*, 2009, **1**, 662–667.
48 X. Wang, X. Tian, Q. Zhang, P. Sun, J. Wu, H. Zhou, B. Jin, J. Yang, S. Zhang, C. Wang, X. Tao, M. Jiang and Y. Tian, *Chem. Mater.*, 2012, **24**, 954–961.
49 R. Indumathy, S. Radhika, M. Kanthimathi, T. Weyhermuller and B. Unni Nair, *J. Inorg. Biochem.*, 2007, **101**, 434–443.
50 B. Zhou, W. Liu, H. Zhang, J. Wu, S. Liu, H. Xu and P. Wang, *Biosens. Bioelectron.*, 2015, **68**, 189–196.
51 G. Song, Y. Sun, Y. Liu, X. Wang, M. Chen, F. Miao, W. Zhang, X. Yu and J. Jin, *Biomaterials*, 2014, **35**, 2103–2112.
52 B. Dumat, G. Bordeau, A. I. Aranda, F. Mahuteau-Betzer, Y. El Harfouch, G. Metge, F. Charra, C. Fiorini-Debuisschert and M. P. Teulade-Fichou, *Org. Biomol. Chem.*, 2012, **10**, 6054–6061.
53 G. Wu, D. H. Robertson, C. L. Brooks III and M. Vieth, *J. Comput. Chem.*, 2003, **24**, 1549–1562.
54 O. P. Cetinkol and N. V. Hud, *Nucleic Acids Res.*, 2009, **37**, 611–621.
55 R. Sinha and G. S. Kumar, *J. Phys. Chem. B*, 2009, **113**, 13410–13420.